ChinaRiceCalendar-Seasonal Crop Calendars for Early, Middle, and Late Rice in China

Hui Li[1], Xiaobo Wang[2,*], Shaoqiang Wang[1,2,3,4,*], Yuanyuan Liu[2], Zhenhai Liu[2], Shiliang Chen[1,2], Qinyi Wang[1], Tongtong Zhu[1], Lunche Wang[1], Lizhe Wang[5]

[1]Key Laboratory of Regional Ecology and Environmental Change, School of Geography and Information Engineering, China University of Geosciences, Wuhan, 430074, China

[2]Key Laboratory of Ecosystem Network Observation and Modeling, Institute of Geographic Sciences and Natural Resources Research, CAS, Beijing, 100101, China

[3]State Key Laboratory of Biogeology and Environmental Geology, China University of Geosciences, Wuhan 430074, China;

[4]College of Resources and Environment, University of Chinese Academy of Sciences, Beijing 100049, China;

[5]Hubei Key Laboratory of Intelligent Geo-Information Processing, China University of Geosciences, Wuhan 430074, China

[*]*Correspondence to: Xiaobo Wang (wxbwxb1995@163.com); Shaoqiang Wang (sqwang@igsnrr.ac.cn)*

Abstract. Long-time series and large-scale rice calendar datasets provide valuable information for agricultural planning and field management in rice-based cropping systems. However, current regional-level rice calendar datasets do not accurately distinguish between rice seasons in China, causing uncertainty in crop model simulation and climate change impact analysis. Based on satellite remote sensing data and an improved PhenoRice algorithm, we extracted the crop areas and phenology of early-, middle-, and late-season rice across China from 2003 to 2020, and established a multi-season rice calendar dataset named ChinaRiceCalendar. Overall, the ChinaRiceCalendar dataset shows a good agreement not only with field-observed rice calendars in Agricultural Meteorological Stations (AMSs), but also with statistical rice areas in various growing seasons. According to the calendar data from 2003 to 2020, the transplanting dates for early, middle, and late rice shifted by +5.4, +2.6, and -5.7 DOY/decade, respectively; the flowering date for early, middle, and late rice shifted by +5.5, -2.8, and -2.7 DOY/decade, respectively; the maturity date for early, middle, and late rice shifted by +3.2, -3.6, and -5.1 DOY/decade, respectively. The ChinaRiceCalendar can be utilized to investigate and optimize the spatio-temporal structure of rice cultivation in China under climate and land-use change.

1 Introduction

As one of the major food crops, rice feeds nearly half of the world's population (Nelson and Gumma, 2015; Fahad et al., 2019). In the context of climate change, continued warming is projected to result in shorter crop growth periods, lower rice productivity, and food insecurity in the Asian monsoon region (Carleton, 2017; Zhao et al., 2017; IPCC, 2022). Revealing changes in rice phenology will facilitate timely adjustment of planting time, rice cultivars, and cropping systems under global warming (Waha et al., 2013; Wang et al., 2022; Wang et al., 2024). Moreover, a dynamic rice calendar with key phenological dates is integral to agricultural monitoring and farmer support systems (Laborte et al., 2017; Fritz et al., 2019; Mishra et al., 2021). Large-scale rice calendars can contribute to more reliable simulations of crop growth and yield at regional and global scales (Franke et al., 2020).

Satellite remote sensing is an effective tool for detecting long-term trends in crop phenology at the regional scale (Xiao et al., 2006; Kotsuki and Tanaka, 2015; Luo et al., 2020; Gao and Zhang, 2021; Mishra et al., 2021). Crop phenology detection methods based on remote sensing vegetation indices (VIs) can be categorized into threshold, inflection point, and shape model approaches. The threshold approaches assume that a development stage begins when the VI value exceeds a predefined threshold (Jönsson et al., 2004; Boschetti et al., 2009; Pan et al., 2015; Guo et al., 2016). The inflection point approaches reconstruct the VI time-series curve by filter smoothing or function fitting, and then corresponds the maxima, minima, and inflection points on the curve to the key phenological events (Zhang et al., 2003; Sakamoto et al., 2005; Sun et al., 2009; Wang et al., 2019). The shape model approaches fit observed VI time-series curves by geometric scaling a robust standard VI time-series curve for the specific crop to identify development stages (Sakamoto et al., 2010; More et al., 2016; Zeng et al., 2016; Sakamoto et al., 2018). In addition to the methods based on time series of VIs, there are also rule-based algorithms that integrate multiple approaches and indicators to detect crop phenology, such as the PhenoRice algorithm proposed by Boschetti et al. (2017). The PhenoRice algorithm, which combines the advantages of threshold and inflection point approaches, utilizes the Enhanced Vegetation Index (EVI), the Normalized Difference Flood Index (NDFI), and the land surface temperature (LST) to estimate rice planting dates. The PhenoRice algorithm excels at extracting rice phenology in multiple cropping systems and has been widely used in East Asia, South Asia, Southeast Asia, and Europe (Busetto et al., 2019; Liu et al., 2020; Mishra et al., 2021). However, the performance of the PhenoRice algorithm depends on the division of rice seasons, which requires expert knowledge about rice-based cropping systems in different regions (Mishra et al., 2021).

In China, there are at least three rice-growing seasons (early, middle, and late seasons) in diverse rice-based cropping systems (e.g., single-rice, double-rice, rice-wheat, rice-rapeseed, and rice-vegetable systems) (Frolking et al., 2002; Qiu et al., 2003; Cao et al., 2021; He et al., 2021). Generally, early-, middle-, and late-season rice are transplanted at Day Of Year (DOY) 30-130, DOY 110–180, and DOY 150-230, respectively. The growth periods after transplanting for early, middle, and late rice are 70-100 days, 100-130 days, and more than 130 days, respectively. Although field observations are important data sources for studying rice calendars in different growing seasons, they are usually limited by spatial and temporal discontinuities (Zhao et al., 2016; Wang et al., 2017). Therefore, previous studies have typically utilized satellite remote sensing products to establish rice calendar datasets at the regional scale (Shihua et al., 2014; Liu et al., 2019; Bai and Xiao, 2020; Luo et al., 2020; Mishra et al., 2021). Nevertheless, these calendar datasets based on satellite remote sensing do not rationally classify rice growing seasons across China. For example, the dataset ChinaCropPhen1km only distinguishes between early and late rice in double-rice systems (Luo et al., 2020); the assumptions of the dataset RICA about rice flowering dates in different seasons do not correspond to the realities in China (Mishra et al., 2021); Shen et al. (2023) produced high-resolution distribution maps of single-season rice but did not explore multiple rice cropping systems. Early-, middle- and late-season rice in China are not only planted at different times, but also have distinguishing varietal characteristics, such as different temperature and photoperiod sensitivities (Zong et al., 2021). Thus, a crop calendar that accurately classifies rice seasons will provide reliable data for agricultural models to calibrate crop parameters at the variety level. Moreover, effective identification of different rice seasons will help analyze the response and adaptation of rice phenology to climate change.

Therefore, to address the shortcomings of the existing rice calendar datasets in China, we attempted to improve the PhenoRice algorithm and use satellite remote sensing data to (1) establish crop calendars for early, middle, and late rice in China; (2) validate the extracted rice areas and calendars in different growing seasons; and (3) explore the spatio-temporal changes of rice calendar dates in major agricultural zones across China from 2003 to 2020.

2 Data and Methodology

2.1 Study area

We selected seven agricultural zones in China as the study area: the Northeast Plain (NP), Huanghuaihai Plain (HP), Loess Plateau (LP), Middle and Lower Yangtze River Region (MLY), South China Region (SC), Yunnan-Guizhou Plateau (YGP), and Sichuan Basin and Surrounding Region (SCS) (Fig. 1). Due to limited hydrothermal resources, the NP and HP zones mainly cultivates single-season rice. Early, middle, and late rice exist in different cropping systems in the MLY zone. The SC zone has a higher cropping frequency than other zones and usually cultivates rice twice a year. Parts of Hainan Province cultivates rice three times a year. Agricultural zoning data were obtained from Resources and Environment Science and Data Center (https://www.resdc.cn/data.aspx?DATAID=275).

2.2 Data

2.2.1 Satellite Imagery

MODIS (Moderate Resolution Imaging Spectroradiometer) remote sensing data are widely used in crop phenology detection because of their excellent performance in temporal and spatial continuity (Reed et al., 1994; Zhang et al., 2003; Zhao et al., 2011; Son et al., 2013). We selected two MODIS EVI products for the study area during 2003–2020: MOD13Q1 (TERRA data) and MYD13Q1 (AQUA data) (https://doi.org/10.5067/MODIS/MOD13Q1.061, 250 m, 16-day). Because the TERRA and AQUA data are based on the synthetic period of moving eight days from each other, the time series of the two 16-day products of MOD13Q1 and MYD13Q1 have a temporal resolution of 8 days (Boschetti et al., 2017). The red (ρ_{RED}) and near-red (ρ_{SWIR}) bands of MOD13Q1 and MYD13Q1 were used to calculate the Normalized Flooding Index (NDFI) (Eq. 1). The Pixel Reliability, Usefulness Index, and Blue Band Reflectance from MOD13Q1/MYD13Q1 were used to assess data quality. In addition, the 1 km spatial resolution and 8-day temporal resolution Land Surface Temperature (LST) product MOD11A2 (https://doi.org/10.5067/MODIS/MOD11A2.061) was employed by resampling 250 m spatial resolution consistent with EVI data.

$$NDFI = \frac{\rho_{RED} - \rho_{SWIR}}{\rho_{RED} + \rho_{SWIR}} \quad (1)$$

All time series data were processed through the Google Earth Engine (GEE) platform and the Python package of Geemap (Wu, 2020).

2.2.2 Validation Data

We obtained the statistical sown areas of rice at the province level during 2003-2020 from the Chinese Agricultural Yearbooks (https://data.cnki.net/yearBook/single?id=N2020120306). We also collected site-scale observations including rice seasons and key phenological dates (transplanting, flowering, and maturity dates) between 2003 and 2013 from 338 Agricultural Meteorological Stations (AMSs, https://data.cma.cn/) in China. Moreover, we compared ChinaRiceCalendar with other regional-scale calendar datasets, including the RiceAtlas dataset based on the agricultural statistics (Laborte et al., 2017), the ChinaCropPhen1km dataset based on the Global Land Surface Satellite (GLASS) leaf area index (LAI) products (Luo et al., 2020), and the RICA dataset based on the MOD13Q1/MYD13Q1 products (Mishra et al., 2021).

2.2.3 Additional Data

Cropland data were obtained from the International Geosphere-Biosphere Program (IGBP) classification of the MODIS land cover product (MCD12Q1) from 2003 to 2020 (https://doi.org/10.5067/MODIS/MCD12Q1.006). Digital elevation model (DEM) data used to create a terrain mask were obtained from the Shuttle Radar Topography Mission (SRTM, https://srtm.csi.cgiar.org). Both data are resampled to a spatial resolution of 250 m.

2.3 Methodology

The technology roadmap of this study is shown in Fig. 2.

2.3.1 Data pre-processing

The data pre-processing in the study falls into three steps:

1. The signal of agronomic flooding was used to help identify the rice transplanting period, but non-agricultural wetlands may have similar flooding signals to paddy fields (Dong and Xiao, 2016; Han et al., 2022). Thus, the annual cropland extent from 2003 to 2020 was used to establish a cropland mask to screen the cropland pixels of the MODIS EVI data.

2. Given that too high an elevation or too great a slope is unsuitable for paddy rice cultivation (Gumma et al., 2011; Dong and Xiao, 2016), only the image pixels with an elevation below 2600 m and a slope less than 8° were selected to extract rice calendars (Han et al., 2022).

3. To reduce the impacts of cloud contamination, we deleted the image pixels with reflectance greater than 0.2 in the blue band (Xiao et al., 2006).

2.3.2 Estimation of rice area and cropping calendar

We combined the PhenoRice algorithm (Boschetti et al., 2017) with a growing season division method (Kong et al., 2022) to extract rice areas and cropping calendars in different growing seasons. Firstly, we identified possible crop flowering periods based on a weighted-smoothed EVI time-series curve in each image pixel. Then we input the possible flowering periods into the PhenoRice algorithm to divide potential growing seasons and check if the corresponding EVI time series belongs to rice. Lastly, we estimated rice planting, flowering, and maturity dates and categorized them into early-, middle-, and late-season calendars according to transplanting time and growing period length.

① **Divide potential growing seasons**: The PhenoRice algorithm requires a pre-specification of rice flowering periods in different growing seasons to extract the corresponding VI time series. To reduce the uncertainty caused by the artificial division of growing seasons, we employed the *phenofit* R package developed by Kong et al. (2022) to identify possible flowering periods in each image pixel. 1) The weighted Whittaker method in the *phenofit* R package was employed to smooth the MODIS-EVI time series (Kong et al., 2022). The Whittaker smoothing function can robustly capture seasonal signals with little noise interference, and it is widely used to identify crop phenology (Atzberger and Eilers, 2011; Bush et al., 2017). The curve fitting mainly relies on information from good-quality points, but also extracts the limited information available from the marginal- and bad-quality points. During the rough fitting to the EVI time series, we categorized the data quality of the observations according to their Quality Control (QC) information (SummaryQA of MOD13A1) and assigned weights of 1.0, 0.5, and 0.2 to the good-, marginal-, and bad-quality VI observations, respectively. 2) Following Kong et al. (2022), the possible flowering date (peak point date) in each crop season was identified by the smoothed EVI time series, based on the rules that only one peak value is inside a growing season and two trough values define a growing season. 3) The possible flowering periods (peak point dates $\pm$ 16 days) detected in each image pixel were input into the PhenoRice algorithm to generate the potential growing seasons.

② **Check if the pixel belongs to a rice-cultivated area**: Whether the pixel belongs to a rice cultivated area during the selected growing season is checked using the following procedure (Boschetti et al., 2017): 1) Compare the observed average, maximum, and minimum EVI values with the corresponding thresholds for paddy fields (EVI_{avg_th}, EVI_{max_th}, *and* EVI_{min_th}) to reduce misclassification problems with evergreen forests and non-vegetative areas; 2) Check for the existence of a maximum inflection point on the EVI curve, which must show a consistent increasing trend before the maxima and a consistent decreasing trend after the maxima. The time interval between the inflection points of the minimum and maximum EVI values during the season must fall within the range of rice vegetative growing periods [*vl1*, *vl2*]; 3) Check if the meteorological conditions on the day of the minimum are favourable for rice crop establishment based on a MODIS-LST value above a specified threshold (LST_{th}); 4) Detect a flood signal (NDFI $\geqslant$ *minndfi*) within a time window (*winfl*) centred on the minimum; 5) Check if there is a consistent increase in EVI observed after the minimum; 6) Check if EVI decreases by more than *decrth*% of the amplitude of the min-max range in a time window after the maxima (*windecr*). Only if all the above requirements are satisfied, the selected growing season in the pixel is labelled as a rice season. The PhenoRice parameters used in the study were calibrated by the phenological observations from the AMSs in China (Table 1).

③ **Estimate rice planting, flowering, and maturity dates**: The rice calendar dates were estimated in the detected rice pixels within the rice seasons. On the EVI time-series curve, the onset date of the field growth period corresponds to the date of the minimum point closest to the retained maximum; the flowering date corresponds to the mid-point date of the period during which the EVI smoothed signal remains above the 90th percentile of the min-max range; the maturity date corresponds to the date when the EVI declined by *decrth*% of the amplitude of the min-max range. Additionally, the study categorized the detected rice calendars into early, middle, and late seasons based on the following rules: 1) the rice with a transplanting date of DOY30-130 and a growing period of 70–100 days was defined as early-season rice; 2) the rice with a transplanting date of DOY110–180 and a growing period of 100–130 days was defined as middle-season rice; 3) the rice with a transplanting date of DOY150-230 and a growing period of 130-150 days was defined as late-season rice.

2.3.3 Data validation

We validated the extracted rice areas during 2003-2020 against the statistics from agricultural yearbooks at the province level. The Chinese Agricultural Yearbooks classify rice varieties into three categories: ER (early rice), MR-SLR (middle rice and single-season late rice), and DLR (double-season late rice). For the consistency of our rice area data with the statistics in variety categorization, we calculated rice planting frequency at the village level and differentiated late rice into single-season late rice and double-season late rice. Due to the difference in spatial resolution between ChinaRiceCalendar and ChinaCropPhen1km, we selected the rice pixels of ChinaRiceCalendar within a one-kilometer radius of the AMSs and the rice pixels of ChinaCropPhen1km within a four-kilometer radius of the AMSs to compare the mean cropping dates in these rice pixels with the corresponding AMS data. Two criteria were used to evaluate the accuracy of the estimated rice areas and cropping dates in each season, namely Root Mean Squared Error (RMSE, Eq. (2)) and R^2 (Eq. (3)):

$$\mathrm{RMSE} = \sqrt{\frac{1}{\mathrm{N}}\sum_{\mathrm{i}=1}^{\mathrm{N}} (\mathrm{true_i} - \mathrm{est_i})^2} \quad (2)$$

$$\mathrm{R}^2 = \left(\frac{\sum_{\mathrm{i}=1}^{\mathrm{N}} (\mathrm{est_i} - \overline{\mathrm{est}})(\mathrm{true_i} - \overline{\mathrm{true}})}{\sqrt{\sum_{\mathrm{i}=1}^{\mathrm{N}} (\mathrm{est_i} - \overline{\mathrm{est}})^2} \sqrt{\sum_{\mathrm{i}=1}^{\mathrm{N}} (\mathrm{true_i} - \overline{\mathrm{true}})^2}} \right)^2 \quad (3)$$

where $\mathrm{true_i}$ is the true value in the ith province or AMS; $\mathrm{est_i}$ is the corresponding estimated value; $\overline{\mathrm{est}}$ and $\overline{\mathrm{true}}$ denote the mean of the estimated and true values, respectively; N is the number of provinces or AMSs.

Additionally, in order to investigate the historical shifts of rice phenological dates in China, we analyzed the trends of rice planting, flowering, and maturity dates at the county level by a Sen+Mann-Kendall trend analysis at a significance level of 0.05. The trend analysis method is detailed in Gocic et al. (2013) .

3 Result

3.1 Validation of rice areas

The detected rice areas during 2003-2020 show a good agreement with statistical sown areas of rice in various growing seasons (Fig. 3). The R^2 between the detected and statistical areas of ER, MR-SLR, and DLR at the province level is 0.92, 0.83, and 0.85, respectively. The RMSE between the detected and statistical areas of ER, MR-SLR, and DLR at the province level is 127.86, 313.06, and 197.47 kha, respectively. The R^2 between the detected and statistical rice areas in different agricultural regions is shown in Table 2. Early rice is mainly distributed in the MLY, SC, SCS, and YGP regions in China and all four regions show high accuracy ($R^2 \in [0.89, 0.97]$) in the detected area of early rice. The NP, HP, and LP regions show higher accuracy ($R^2 \in [0.93, 0.95]$) than the SCS, MLY, SC, and YGP regions ($R^2 \in [0.73, 0.82]$) in the detected area of middle rice and single-season late rice. Moreover, the MLY and YGP regions have more reliable data ($R^2 \in [0.85, 0.89]$) on the area of double-season late rice than the SC and SCS regions ($R^2 \in [0.78, 0.79]$).

3.2 Validation of rice calendars

Overall, the key phenological dates estimated in the study show high consistency with the data from AMSs (Fig. 4). The R^2 between data from ChinaRiceCalendar and AMSs for transplanting, flowering, and maturity dates in China is 0.95, 0.95, and 0.96, respectively. The RMSE between data from ChinaRiceCalendar and AMSs for transplanting, flowering, and maturity dates in China is 8.34, 7.84, and 7.77 days, respectively. Moreover, the error in detected middle-rice calendars is lower than that in early-rice and late-rice calendars (Fig. 4). The RMSE of the estimated transplanting, flowering, and maturity dates for early rice is 8.82, 8.27, and 10.77 days, respectively. The RMSE of the estimated transplanting, flowering, and maturity dates for middle rice is 7.44, 6.53, and 5.14 days, respectively. The RMSE of the estimated transplanting, flowering, and maturity dates for late rice is 8.28, 9.07, and 10.06 days, respectively.

Also, we calculated the RMSE of the estimated rice cropping dates in the seven agricultural regions in China (Fig. 5). Except in the SC region, the RMSE averages of the estimated phenological dates are around one week at the regional scale. For early-season rice, the RMSE average of the estimated cropping dates is 6.76, 13.54, and 7.30 days in the MLY, SC, and YGP, respectively. For middle-season rice, the range of the RMSEs in the seven agricultural regions is from 5.46 days in the NP to 7.81 days in the SC. For late-season rice, the RMSE average of the estimated cropping dates is 8.60, 10.08, and 8.29 days in the MLY, SC, and YGP, respectively.

3.3 Comparison with other calendar datasets

The rice phenological dates obtained from the RiceAtlas (Laborte et al., 2017), ChinaCropPhen1km (Luo et al., 2020), and RICA (Mishra et al., 2021) datasets were also validated against the spatially corresponding AMS data. In China, the rice phenological dates estimated in ChinaRiceCalendar show higher accuracy by growing season than those obtained from RiceAtlas and RICA. Furthermore, compared to the ChinaCropPhen1km dataset, the ChinaRiceCalendar dataset have similar accuracy in rice phenological dates but higher accuracy in rice areas in different growing seasons.

The RMSE between RiceAtlas' and AMSs' phenological dates for early, middle, and late rice in China is 18.27, 21.03, and 13.81 days, respectively. The R^2 between RiceAtlas' and AMSs' phenological dates for early, middle, and late rice in China is 0.65, 0.43, and 0.75, respectively.

The RMSE between ChinaCropPhen1km's and AMSs' phenological dates is 9.35 days for early and middle rice, and 7.24 days for late rice in China. The R^2 between ChinaCropPhen1km's and AMSs' phenological dates is 0.81 for early and middle rice, and 0.85 for late rice in China.

The RMSE between RICA's and AMSs' phenological dates for early, middle, and late rice in China is 22.80, 14.07, and 13.61 days, respectively. The R^2 between RICA's and AMSs' phenological dates for early, middle, and late rice in China is 0.47, 0.69, and 0.73, respectively.

3.4 Spatial distribution of rice areas and phenological dates

According to the spatial distribution of the detected rice areas during 2003-2020, early and late rice were mainly grown in the southern part of China, while middle rice was widely planted in China from south to north (Fig. 6). Based on the mean values between 2003 and 2020, the detected planting area of early rice in China was 4732 kha, and approximately 69% of the early-rice area was concentrated in the MLY region; the detected planting area of middle rice in China was 13953 kha, and approximately 85% of the middle-rice area was distributed in the MLY, NP, and SCS regions; the detected planting area of single-season late rice in China was 4361 kha, and approximately 70% of the single-season late rice area was distributed in the MLY region; the detected planting area of double-season late rice in China was 6423 kha, and approximately 64% of the double-season late rice area was distributed in the MLY region.

The spatial variations of rice phenology are significant in early, middle, and late seasons (Fig. 7 and 8). In the NP, HP, and LP, middle rice was transplanted at DOY130±21, flowered at DOY200±14, and matured at DOY260±14. In the YGP, the mean transplanting date was approximately DOY60 for early rice, DOY125 for middle rice, and DOY150 for late rice; the mean flowering date for early, middle, and late rice was DOY180±30; the mean maturity date was approximately DOY180 for early rice, DOY250 for middle rice, and DOY290 for late rice. In the MLY, the mean transplanting date was approximately DOY110 for early rice, DOY160 for middle rice, and DOY170 for late rice; the mean flowering date was approximately DOY160 for early rice, DOY220 for middle rice, and DOY250 for late rice; the mean maturity date was DOY280±21 for the three seasons. In the SC, the mean transplanting date was approximately DOY90 for early rice and DOY180 for late rice; the mean flowering date was approximately DOY180 for early rice and DOY240 for late rice; the mean maturity date was approximately DOY210 for early rice and DOY300 for late rice.

3.5 Temporal changes in rice phenological dates

Based on the trend analysis of rice phenological dates from 2003 to 2020 (Fig. 9), the transplanting dates for early, middle, and late rice shifted by +5.4, +2.6, and -5.7 DOY/decade, respectively; the flowering date for early, middle, and late rice shifted by +5.5, -2.8, and -2.7 DOY/decade, respectively;

the maturity date for early, middle, and late rice shifted by +3.2, -3.6, and -5.1 DOY/decade, respectively. According to the trend analysis result in each rice-producing county in China between 2003 and 2020 (Fig. 10), 27%, 12%, and 3% of the counties showed a significant delay in transplanting dates for early, middle, and late rice, respectively; meanwhile, 5%, 6%, and 25% of the counties showed a significant advancement in transplanting dates for early, middle, and late rice, respectively. Moreover, 27%, 9%, and 1% of the counties in China showed a significant delay in flowering dates for early, middle, and late rice, respectively; meanwhile, 1%, 7%, and 22% of the counties showed a significant advancement in flowering dates for early, middle, and late rice, respectively. Also, 24%, 6%, and 2% of the counties in China showed a significant delay in maturity dates for early, middle, and late rice, respectively; meanwhile, 2%, 14%, and 19% of the counties showed a significant advancement in flowering dates for early, middle, and late rice, respectively. Overall, the growing season of early rice tended to be delayed, while the growing season of late rice tended to advance between 2003 and 2020 in China. Additionally, the shifts in the phenological dates of middle rice during 2003-2020 depended on the agricultural region (Fig. 10).

4 Uncertainties in ChinaRiceCalendar

Although the generated dataset ChinaRiceCalendar shows an advantage in rice season identification, there is still uncertainty in the data source and phenology detection methods.

This study used MODIS remote sensing data to extract rice phenological dates in various growing seasons in China. The MODIS remote sensing products have an appropriate temporal resolution, long time series, and good time consistency for analyzing changes in rice calendars at the regional scale. Moreover, the MODIS data are easy to obtain and process on the GEE platform, allowing for automated and timely updating of the calendar dataset. However, the pixel-based detection of rice areas may be interfered with by the contamination of clouds, aerosols, and water vapor, especially during the monsoon season when rice is by far the dominant crop (Xiao et al., 2014; Mishra et al., 2021). Because synthetic aperture radar (SAR) can penetrate through clouds, subsequent studies could combine optical and SAR images to avoid the impacts of clouds (Shen et al., 2023). Also, most paddies in southern China are smaller than the spatial resolution of MODIS data, which may result in a rough estimation of rice areas. Generating more satellite remote sensing products with higher spatial resolution and integrating multiple data sources from satellite-airborne-ground observations will facilitate real-time monitoring of rice cropping areas at the regional scale (Zheng et al., 2022; Sun et al., 2023). Additionally, precisely corresponding the image pixels from the MODIS dataset to the Agricultural Meteorological Stations remains a challenge during data validation. In the future, it would be beneficial to conduct a quantitative assessment to determine the representativeness of the MODIS pixels surrounding the AMS site.

In this study, we improved the method of growing season division in the PhenoRice algorithm. We also attempted to remove non-paddy pixels and reduce the impacts of low-quality data on the reconstruction of EVI time-series curves. Nevertheless, since the PhenoRice algorithm detects rice pixels by agronomic flooding signals, rainfed or upland rice systems will be much harder to detect. In China, rice is mainly planted in flooded paddy fields (Luo et al., 2022), which mitigates the problems of detecting rainfed or upland rice. Moreover, the VI-curve smoothing methods perform differently in different regions (Luo et al., 2020). To enhance the identification of rice growing seasons in multi-cropping areas, we suggested identifying the optimal smoothing method for MODIS-EVI time series in various rice-based cropping systems. Although the local tuning of the PhenoRice algorithm parameters could further improve the results, we employed a single configuration of temporal windows and threshold values across China because automated methods that perform robustly are essential for developing timely information about crop calendars over large extents (Mishra et al., 2021).

The uncertainty in crop area estimation is more significant for late rice than for early and middle rice, resulting in lower accuracy of the detected rice area in southern China (MLY, SC, SCS, YGP) than in northern China (NP, HP, LP). For example, there is an underestimation of the double-season late rice area in Hainan Province and an overestimation of the single-season late rice area in Hubei Province. Because the transplanting dates (DOY150-210) of late rice coincide with the rainy season in the main rice-producing areas, there is a higher risk of misidentifying agronomic flooding signals during transplanting for late rice than for early and middle rice. Furthermore, low data quality induced by cloud contamination during the transplanting period contributes to the difficulties in extracting the late rice area (Xiao et al., 2005; Clauss et al., 2016). Also, the diverse multi-cropping systems and the complex growing environments (e.g., topography and landscape) make the area detection for late rice more challenging (Dong and Xiao, 2016). The following study could consider utilizing geostationary satellite observations to increase the temporal frequency of remote sensing data during the transplantation period of late rice in China (Shen et al., 2023). Subsequently, we will try to automate the generation of ChinaRiceCalendar based on the 'rgee' package (Aybar et al., 2023) and update the database once a year.

5 Data Availability

ChinaRiceCalendar is a raster dataset with 250m, 1km, and 10km spatial resolution. The spatial reference system of the dataset is Asia_North_Albers_Equal_Area_Conic. The dataset currently covers the following periods: 2003-2010, 2011-2015, and 2016-2020. ChinaRiceCalendar is available at https://doi.org/10.7910/DVN/EUP8EY (Hui Li, 2023).

6 Conclusions

In the study, we improved the procedure of growing season division in the PhenoRice algorithm, and detected rice areas and rice phenology in early, middle, and late seasons across China from 2003 to 2020. Then, we established a multi-season rice calendar dataset named ChinaRiceCalendar. Firstly, the detected rice areas in ChinaRiceCalendar show a good agreement with statistical sown areas of rice in various growing seasons. The R^2 between the detected and statistical areas of ER, MR-SLR, and DLR at the province level is 0.92, 0.83, and 0.85, respectively. Secondly, the key phenological dates in ChinaRiceCalendar have high consistency with the field observations from 338 Agricultural Meteorological Stations in China. The RMSE between data from ChinaRiceCalendar and AMSs for rice transplanting, flowering, and maturity dates in China is 8.34, 7.84, and 7.77 days, respectively. Thirdly, ChinaRiceCalendar shows higher accuracy in the detected rice area or key phenological dates by growing season than RiceAtlas, ChinaCropPhen1km, and RICA in China. According to the calendar data from 2003 to 2020, the transplanting dates for early, middle, and late rice shifted by +5.4, +2.6, and -5.7 DOY/decade, respectively; the flowering date for early, middle, and late rice shifted by +5.5, -2.8, and -2.7 DOY/decade, respectively; the maturity date for early, middle, and late rice shifted by +3.2, -3.6, and -5.1 DOY/decade, respectively. Overall, ChinaRiceCalendar provides more reliable data to investigate and optimize the spatio-temporal structure of rice cultivation in China under climate and land-use change.

Author Contributions: Conceptualization, methodological and algorithmic improvements, HL and XW; data download and processing, YL and ZL; validation, SC and QW; formal analysis, HL, XW, and TZ; writing-original draft preparation, HL and XW; writing-review and editing, XW, SW and LW. All authors have read and agreed to the published version of the manuscript.

Financial support: This research has been supported by the National Natural Science Foundation of China (Project Nos. 31861143015 and 32301393).

Acknowledgments: We would like to thank Dongdong Kong from China University of Geosciences (Wuhan) for providing the R package *Phnofit* and thank Mirco Boschetti from the Italian National Research Council for providing the source code of *PhenoRice.*

Conflicts of Interest: The authors declare no conflict of interest.

References

Atzberger, C. and Eilers, P.H.: Evaluating the effectiveness of smoothing algorithms in the absence of ground reference measurements. International Journal of Remote Sensing, 32(13), 3689-3709, 2011.

Aybar, C. rgee: R Bindings for Calling the 'Earth Engine' API (Version 1.1.7). https://github.com/r-spatial/rgee/issues/, 2023.

Bai, H. and Xiao, D.: Spatiotemporal changes of rice phenology in China during 1981 – 2010. Theoretical and Applied Climatology, 140, 1483-1494, 2020.

Boschetti, M., Busetto, L., Manfron, G., Laborte, A., Asilo, S., Pazhanivelan, S. and Nelson, A.: PhenoRice: A method for automatic extraction of spatio-temporal information on rice crops using satellite data time series. Remote sensing of environment, 194, 347-365, 2017.

Boschetti, M., Stroppiana, D., Brivio, P. and Bocchi, S.: Multi-year monitoring of rice crop phenology through time series analysis of MODIS images. International journal of remote sensing, 30(18), 4643-4662, 2009.

Busetto, L., Zwart, S.J. and Boschetti, M.: Analysing spatial – temporal changes in rice cultivation practices in the Senegal River Valley using MODIS time-series and the PhenoRice algorithm. International Journal of Applied Earth Observation and Geoinformation, 75, 15-28, 2019.

Bush, E.R., Abernethy, K.A., Jeffery, K., Tutin, C., White, L., Dimoto, E., Dikangadissi, J.T., Jump, A.S. and Bunnefeld, N.: Fourier analysis to detect phenological cycles using long - term tropical field data and simulations. Methods in Ecology and Evolution, 8(5), 530-540, 2017.

Cao, J., Cai, X., Tan, J., Cui, Y., Xie, H., Liu, F., Yang, L. and Luo, Y.: Mapping paddy rice using Landsat time series data in the Ganfu Plain irrigation system, Southern China, from 1988– 2017. International Journal of Remote Sensing, 42(4), 1556-1576, 2021.

Carleton, T.A.: Crop-damaging temperatures increase suicide rates in India. Proceedings of the National Academy of Sciences, 114(33), 8746-8751, 2017.

Clauss, K., Yan, H. and Kuenzer, C.: Mapping paddy rice in China in 2002, 2005, 2010 and 2014 with MODIS time series. Remote Sensing, 8(5), 434, 2016.

Dong, J. and Xiao, X.: Evolution of regional to global paddy rice mapping methods: A review. ISPRS Journal of Photogrammetry and Remote Sensing, 119, 214-227, 2016.

Fahad, S., Adnan, M., Noor, M., Arif, M., Alam, M., Khan, I.A., Ullah, H., Wahid, F., Mian, I.A. and Jamal, Y.: Major constraints for global rice production, Advances in rice research for abiotic stress tolerance. Elsevier, pp. 1-22, 2019.

Franke, J.A., Müller, C., Elliott, J., Ruane, A.C., Jägermeyr, J., Snyder, A., Dury, M., Falloon, P.D., Folberth, C. and François, L.: The GGCMI Phase 2 emulators: global gridded crop model responses to changes in CO 2, temperature, water, and nitrogen (version 1.0). Geoscientific Model Development, 13(9), 3995-4018, 2020.

Fritz, S., See, L., Bayas, J.C.L., Waldner, F., Jacques, D., Becker-Reshef, I., Whitcraft, A., Baruth, B., Bonifacio, R. and Crutchfield, J.: A comparison of global agricultural monitoring systems and current gaps. Agricultural systems, 168, 258-272, 2019.

Frolking, S., Qiu, J., Boles, S., Xiao, X., Liu, J., Zhuang, Y., Li, C. and Qin, X.: Combining remote sensing and ground census data to develop new maps of the distribution of rice agriculture in China. Global Biogeochemical Cycles, 16(4), 38-1-38-10, 2002.

Gao, F. and Zhang, X.: Mapping crop phenology in near real-time using satellite remote sensing: Challenges and opportunities. Journal of Remote Sensing, 2021, 2021.

Gocic, M. and Trajkovic, S.: Analysis of changes in meteorological variables using Mann-Kendall and Sen's slope estimator statistical tests in Serbia. Global and Planetary Change, 100, 172-182, 2013.

Gumma, M.K., Nelson, A., Thenkabail, P.S. and Singh, A.N.: Mapping rice areas of South Asia using MODIS multitemporal data. Journal of applied remote sensing, 5(1), 053547, 2011.

Guo, L., An, N. and Wang, K.: Reconciling the discrepancy in ground-and satellite-observed trends in the spring phenology of winter wheat in China from 1993 to 2008. Journal of Geophysical Research: Atmospheres, 121(3), 1027-1042, 2016.

Han, J., Zhang, Z., Luo, Y., Cao, J., Zhang, L., Zhuang, H., Cheng, F., Zhang, J. and Tao, F.: Annual paddy rice planting area and cropping intensity datasets and their dynamics in the Asian monsoon region from 2000 to 2020. Agricultural Systems, 200, 103437, 2022.

He, Y., Dong, J., Liao, X., Sun, L., Wang, Z., You, N., Li, Z. and Fu, P.: Examining rice distribution and cropping intensity in a mixed single-and double-cropping region in South China using all available Sentinel 1/2 images. International Journal of Applied Earth Observation and Geoinformation, 101, 102351, 2021.

Hui Li, Xiaobo Wang, Shaoqiang Wang, Yuanyuan Liu, Zhenhai Liu, Shiliang Chen, Qinyi Wang, Tongtong Zhu, Lunche Wang, Lizhe Wang. ChinaRiceCalendar. Harvard Dataverse, doi/10.7910/DVN/EUP8EY, 2023.

IPCC. Climate change 2022: impacts, adaptation and vulnerability. https://www.ipcc.ch/report/sixth-assessment-report-working-group-ii/, 2022.

Kim, D.-H., Jang, T., Hwang, S., and Jeong, H.: Paddy rice adaptation strategies to climate change: Transplanting date shift and BMP applications, Agricultural Water Management, 252, 106926, 2021.

Kong, D., McVicar, T.R., Xiao, M., Zhang, Y., Peña‐Arancibia, J.L., Filippa, G., Xie, Y. and Gu, X.: phenofit: An R package for extracting vegetation phenology from time series remote sensing. Methods in Ecology and Evolution, 2022.

Kotsuki, S. and Tanaka, K.: SACRA – a method for the estimation of global high-resolution crop calendars from a satellite-sensed NDVI. Hydrology and Earth System Sciences, 19(11), 4441-4461, 2015.

Laborte, A.G., Gutierrez, M.A., Balanza, J.G., Saito, K., Zwart, S.J., Boschetti, M., Murty, M., Villano, L., Aunario, J.K. and Reinke, R.: RiceAtlas, a spatial database of global rice calendars and production. Scientific data, 4(1), 1-10, 2017.

Liu, L., Huang, J., Xiong, Q., Zhang, H., Song, P., Huang, Y., Dou, Y. and Wang, X.: Optimal MODIS data processing for accurate multi-year paddy rice area mapping in China. GIScience & Remote Sensing, 57(5), 687-703, 2020.

Liu, Y., Zhou, W. and Ge, Q.: Spatiotemporal changes of rice phenology in China under climate change from 1981 to 2010. Climatic Change, 157, 261-277, 2019.

Luo, W., Chen, M., Kang, Y., Li, W., Li, D., Cui, Y., Khan, S. and Luo, Y.: Analysis of crop water requirements and irrigation demands for rice: Implications for increasing effective rainfall. Agricultural Water Management, 260, 107285, 2022.

Luo, Y., Zhang, Z., Chen, Y., Li, Z. and Tao, F.: ChinaCropPhen1km: a high-resolution crop phenological dataset for three staple crops in China during 2000–2015 based on leaf area index (LAI) products. Earth System Science Data, 12(1), 197-214, 2020.

Mishra, B., Busetto, L., Boschetti, M., Laborte, A. and Nelson, A.: RICA: A rice crop calendar for Asia based on MODIS multi year data. International Journal of Applied Earth Observation and Geoinformation, 103, 102471, 2021.

More, R.S., Manjunath, K., Jain, N.K., Panigrahy, S. and Parihar, J.S.: Derivation of rice crop calendar and evaluation of crop phenometrics and latitudinal relationship for major south and south-east Asian countries: A remote sensing approach. Computers and Electronics in Agriculture, 127, 336-350, 2016.

Nelson, A. and Gumma, M.: A map of lowland rice extent in the major rice growing countries of Asia. IRRI, Los Banos, Philippines, 2015.

Pan, Z., Huang, J., Zhou, Q., Wang, L., Cheng, Y., Zhang, H., Blackburn, G.A., Yan, J. and Liu, J.: Mapping crop phenology using NDVI time-series derived from HJ-1 A/B data. International Journal of Applied Earth Observation and Geoinformation, 34, 188-197, 2015.

Parmesan, C., Morecroft, M.D. and Trisurat, Y.: Climate change 2022: Impacts, adaptation and vulnerability, GIEC, 2022.

Qiu, J., Tang, H., Frolking, S., Boles, S., Li, C., Xiao, X., Liu, J., Zhuang, Y. and Qin, X.: Mapping single-, double-, and triple-crop agriculture in China at 0.5°× 0.5° by combining county-scale census data with a remote sensing-derived land cover map. Geocarto International, 18(2), 3-13, 2003.

Reed, B.C., Brown, J.F., VanderZee, D., Loveland, T.R., Merchant, J.W. and Ohlen, D.O.: Measuring phenological variability from satellite imagery. Journal of vegetation science, 5(5), 703-714, 1994.

Sakamoto, T., Wardlow, B.D., Gitelson, A.A., Verma, S.B., Suyker, A.E. and Arkebauer, T.J.: A two-step filtering approach for detecting maize and soybean phenology with time-series MODIS data. Remote Sensing of Environment, 114(10), 2146-2159, 2010.

Sakamoto, T., Yokozawa, M., Toritani, H., Shibayama, M., Ishitsuka, N. and Ohno, H.: A crop phenology detection method using time-series MODIS data. Remote sensing of environment, 96(3-4), 366-374, 2005.

Sakamoto, T.: Refined shape model fitting methods for detecting various types of phenological information on major US crops. ISPRS Journal of Photogrammetry and Remote Sensing, 138, 176-192, 2018.

Shen, R., Pan, B., Peng, Q., Dong, J., Chen, X., Zhang, X., Ye, T., Huang, J. and Yuan, W.: High-resolution distribution maps of single-season rice in China from 2017 to 2022. Earth System Science Data Discussions, 1-27, 2023.

Shen, Y., Zhang, X., Yang, Z., Ye, Y., Wang, J., Gao, S., Liu, Y., Wang, W., Tran, K.H. and Ju, J.: Developing an operational algorithm for near-real-time monitoring of crop progress at field scales by fusing harmonized Landsat and Sentinel-2 time series with geostationary satellite observations. Remote Sensing of Environment, 296, 113729, 2023.

Shihua, L., Jingtao, X., Ping, N., Jing, Z., Hongshu, W. and Jingxian, W.: Monitoring paddy rice phenology using time series MODIS data over Jiangxi Province, China. International Journal of Agricultural and Biological Engineering, 7(6), 28-36, 2014.

Son, N.-T., Chen, C.-F., Chen, C.-R., Duc, H.-N. and Chang, L.-Y.: A phenology-based classification of time-series MODIS data for rice crop monitoring in Mekong Delta, Vietnam. Remote Sensing, 6(1), 135-156, 2013.

Sun, C., Zhang, H., Xu, L., Ge, J., Jiang, J., Zuo, L. and Wang, C.: Twenty-meter annual paddy rice area map for mainland Southeast Asia using Sentinel-1 synthetic-aperture-radar data. Earth System Science Data, 15(4), 1501-1520, 2023.

Sun, H., Huang, J. and Peng, D.: Detecting major growth stages of paddy rice using MODIS data. J. Remote Sens, 13, 1122-1137, 2009.

Waha, K., Müller, C. and Rolinski, S.: Separate and combined effects of temperature and precipitation change on maize yields in sub-Saharan Africa for mid-to late-21st century. Global and Planetary Change, 106, 1-12, 2013.

Wang, J., Yu, K., Tian, M. and Wang, Z.: Estimation of rice key phenology date using Chinese HJ-1 vegetation index time-series images, 2019 8th International Conference on Agro-Geoinformatics (Agro-Geoinformatics). IEEE, pp. 1-4, 2019.

Wang, X., Ciais, P., Li, L., Ruget, F., Vuichard, N., Viovy, N., Zhou, F., Chang, J., Wu, X. and Zhao, H.: Management outweighs climate change on affecting length of rice growing period for early rice and single rice in China during 1991–2012. Agricultural and Forest Meteorology, 233, 1-11, 2017.

Wang, X., Folberth, C., Skalsky, R., Wang, S., Chen, B., Liu, Y., Chen, J. and Balkovic, J.: Crop calendar optimization for climate change adaptation in rice-based multiple cropping systems of India and Bangladesh. Agricultural and Forest Meteorology, 315, 108830, 2022.

Wang, X., Wang, S., Folberth, C., Skalsky, R., Li, H., Liu, Y. and Balkovic, J.: Limiting global warming to 2°C benefits building climate resilience in rice-wheat systems in India through crop calendar management. Agricultural Systems, 213, 103806, 2024.

Wu, Q.: geemap: A Python package for interactive mapping with Google Earth Engine. Journal of Open Source Software, 5(51), 2305, 2020.

Xiao, X., Boles, S., Frolking, S., Li, C., Babu, J.Y., Salas, W. and Moore III, B.: Mapping paddy rice agriculture in South and Southeast Asia using multi-temporal MODIS images. Remote sensing of Environment, 100(1), 95-113, 2006.

Xiao, X., Boles, S., Liu, J., Zhuang, D., Frolking, S., Li, C., Salas, W. and Moore III, B.: Mapping paddy rice agriculture in southern China using multi-temporal MODIS images. Remote sensing of environment, 95(4), 480-492, 2005.

Zeng, L., Wardlow, B.D., Wang, R., Shan, J., Tadesse, T., Hayes, M.J. and Li, D.: A hybrid approach for detecting corn and soybean phenology with time-series MODIS data. Remote Sensing of Environment, 181, 237-250, 2016.

Zhang, X., Friedl, M.A., Schaaf, C.B., Strahler, A.H., Hodges, J.C., Gao, F., Reed, B.C. and Huete, A.: Monitoring vegetation phenology using MODIS. Remote sensing of environment, 84(3), 471-475, 2003.

Zhang, Z., Song, X., Tao, F., Zhang, S. and Shi, W.: Climate trends and crop production in China at county scale, 1980 to 2008. Theoretical and Applied Climatology, 123(1), 291-302, 2016.

Zhao, C., Liu, B., Piao, S., Wang, X., Lobell, D.B., Huang, Y., Huang, M., Yao, Y., Bassu, S. and Ciais, P.: Temperature increase reduces global yields of major crops in four independent estimates. Proceedings of the National Academy of sciences, 114(35), 9326-9331, 2017.

Zhao, H., Yang, Z., Di, L. and Pei, Z.: Evaluation of temporal resolution effect in remote sensing based crop phenology detection studies, International Conference on Computer and Computing Technologies in Agriculture. Springer, pp. 135-150, 2011.

Zheng, J., Song, X., Yang, G., Du, X., Mei, X. and Yang, X.: Remote sensing monitoring of rice and wheat canopy nitrogen: A review. Remote Sensing, 14(22), 5712, 2022.

Zong, W., Ren, D., Huang, M., Sun, K., Feng, J., Zhao, J., Xiao, D., Xie, W., Liu, S. and Zhang, H.: Strong photoperiod sensitivity is controlled by cooperation and competition among Hd1, Ghd7 and DTH8 in rice heading. New Phytologist, 229(3), 1635-1649, 2021.

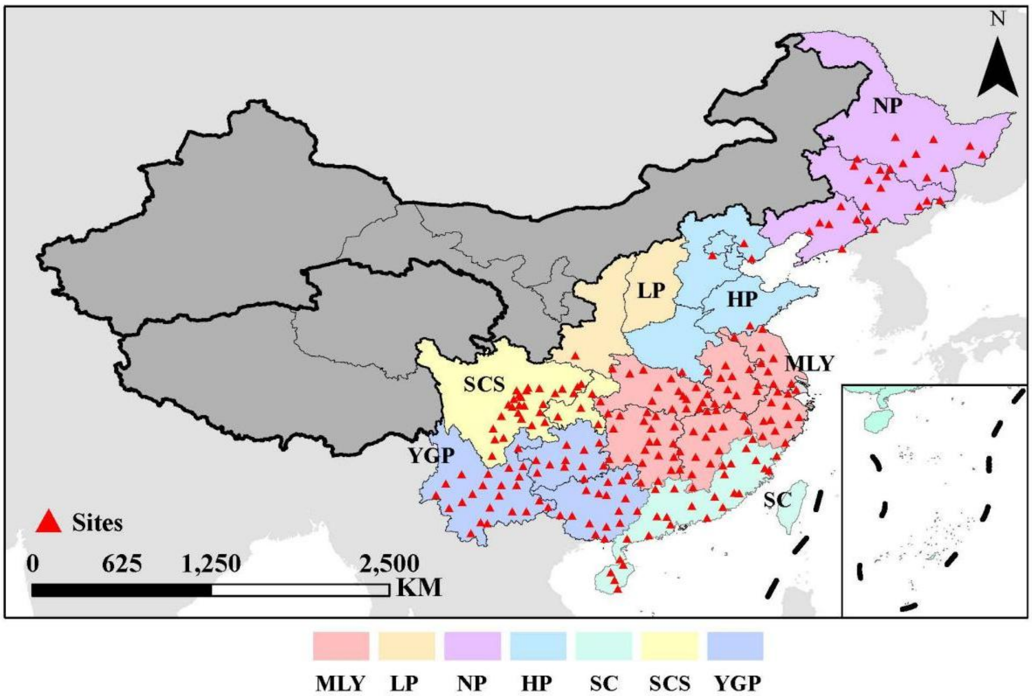

Fig.1 Study area and distribution of Agricultural Meteorological Stations (AMSs) in China

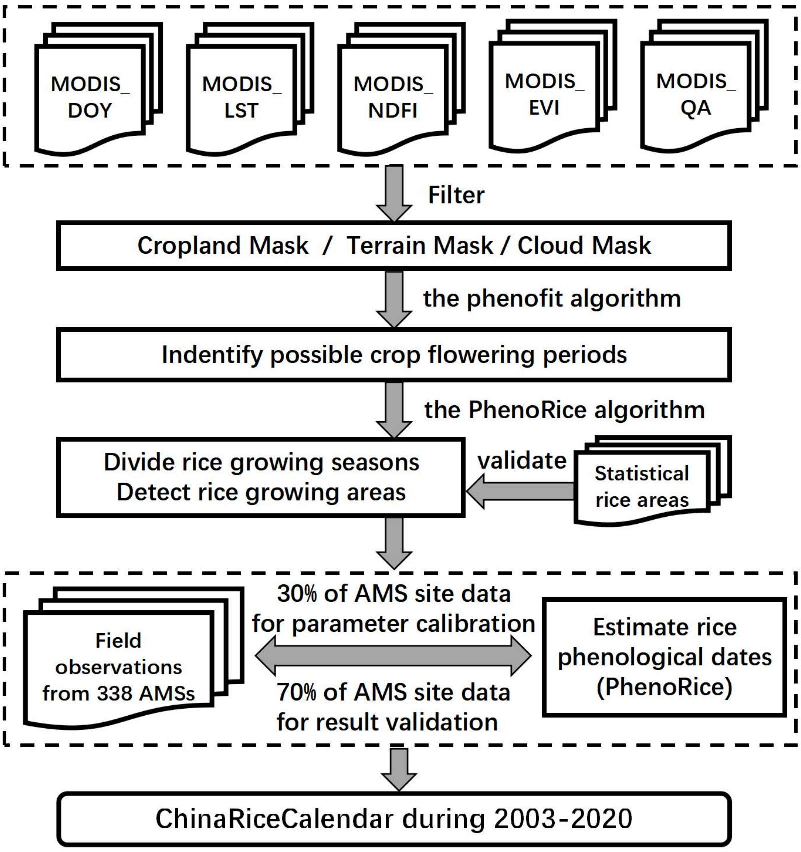

Fig.2 Technology roadmap for this study

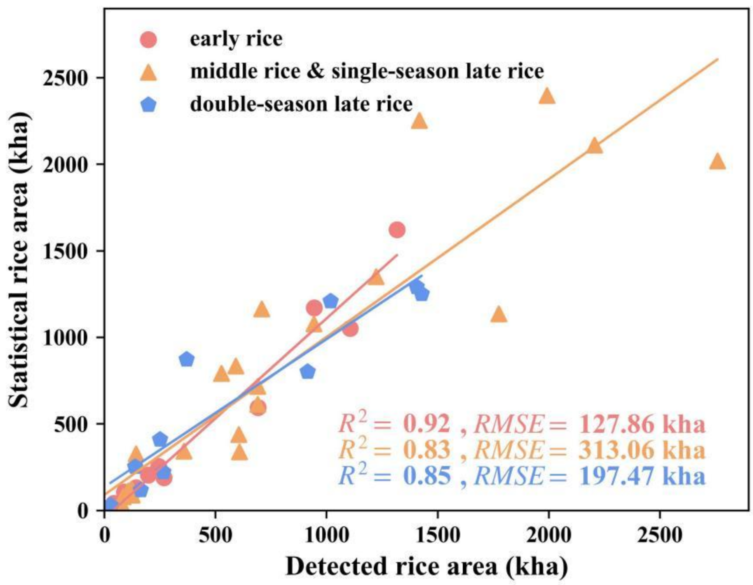

Fig.3 Comparison between detected and statistical rice areas at the province scale (red dots represent early rice, orange squares represent middle rice and single-season late rice, blue pentagons represent double-season late rice)

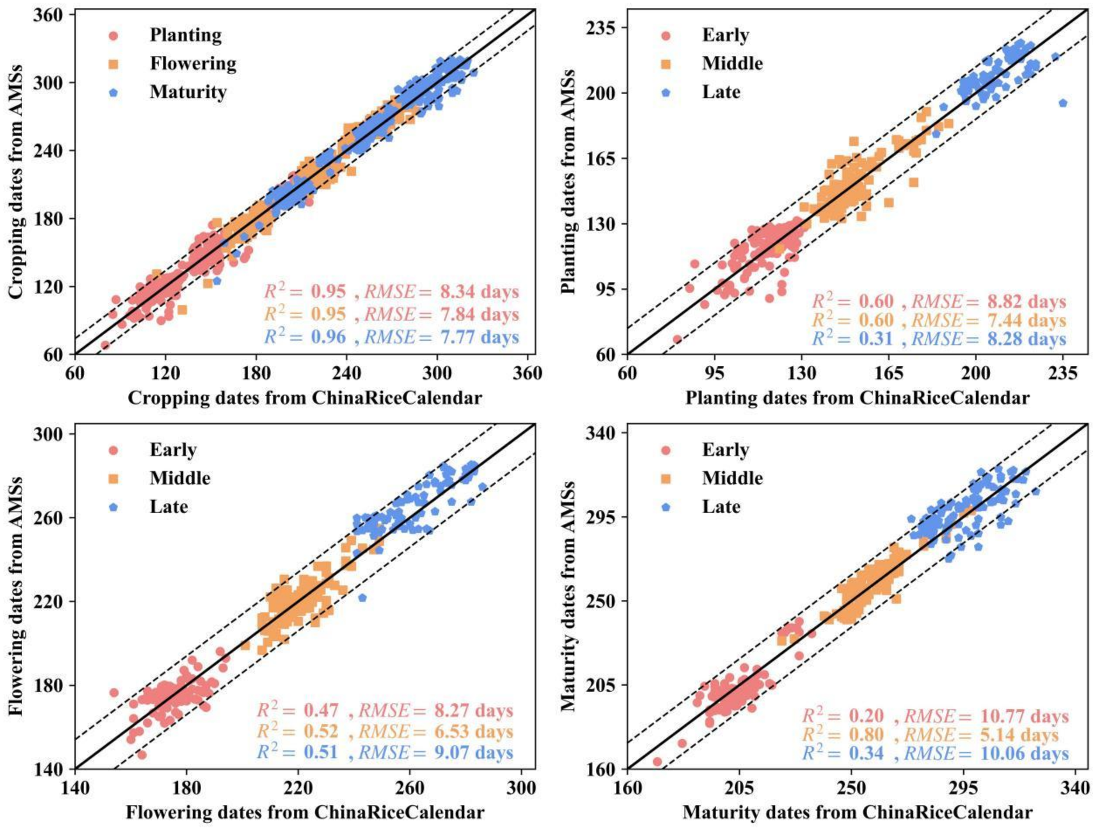

Fig.4 Comparison of rice phenological dates between ChinaRiceCalendar and AMS data at the site scale (dashed lines are ±14 days)

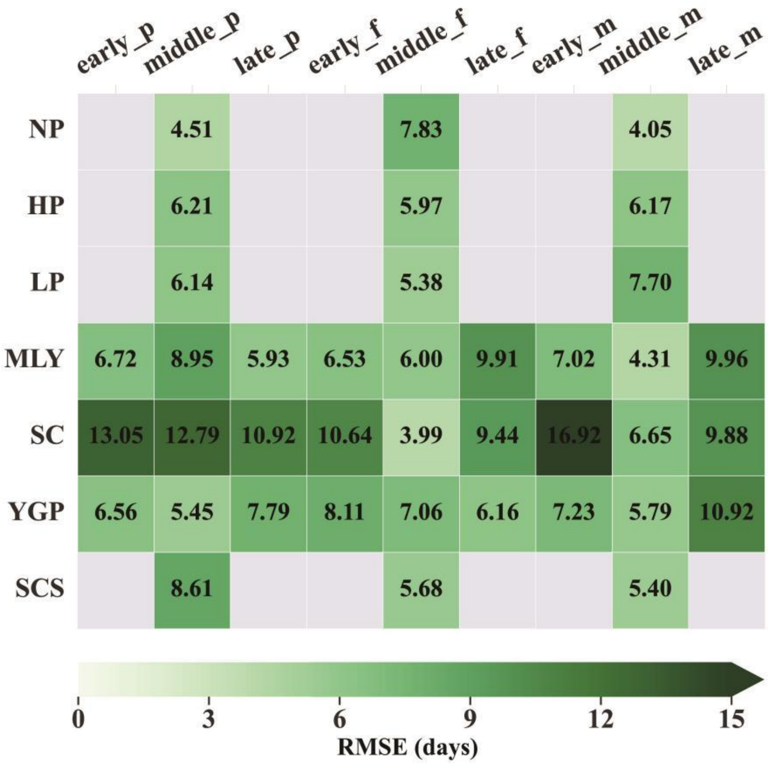

Fig.5 RMSEs of rice phenological dates between ChinaRiceCalendar and AMS data in main agricultural regions

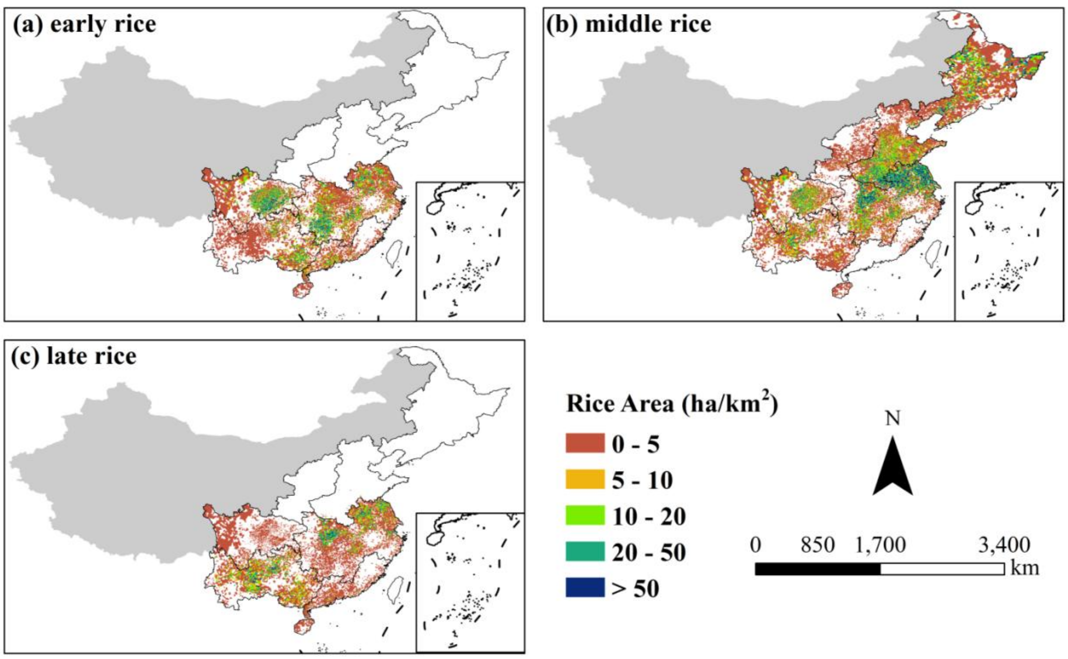

Fig.6 Spatial distribution of rice areas in China during 2003-2020 (a: early rice, b: middle rice, c: late rice)

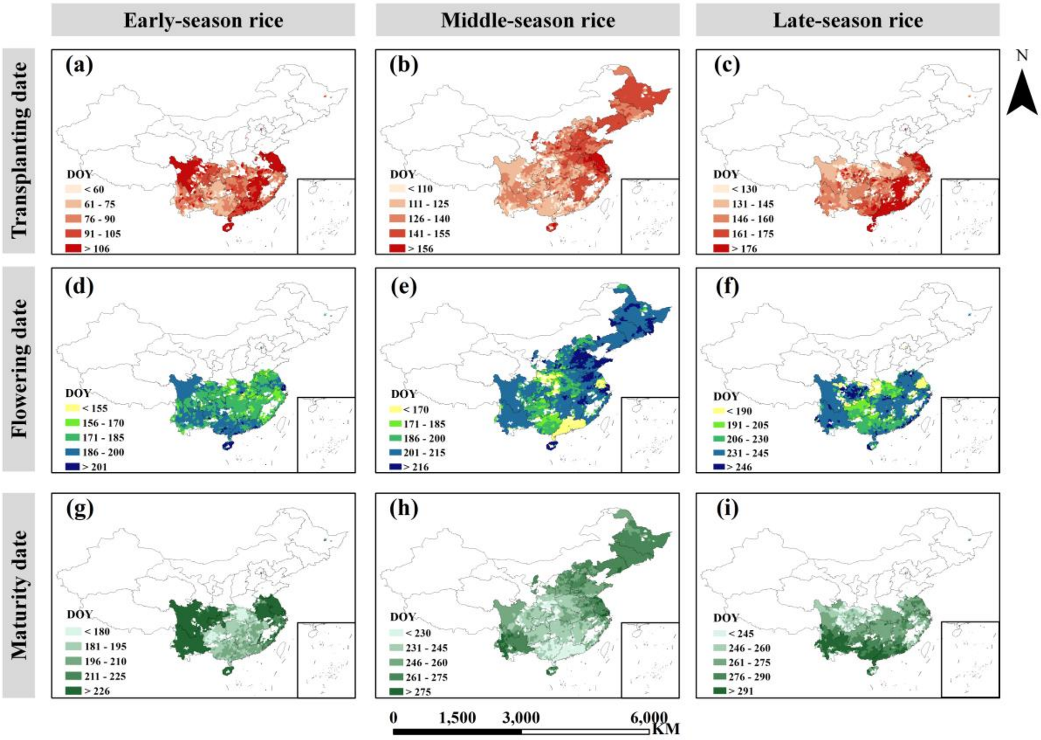

Fig.7 Rice phenological dates at the county scale between 2003 and 2020 (a: early-rice transplanting dates; b: middle-rice transplanting dates; c: late-rice transplanting dates; d: early-rice flowering dates; e: middle-rice flowering dates; f: late-rice flowering dates; g: early-rice maturity dates; h: middle-rice maturity dates; i: late-rice maturity dates)

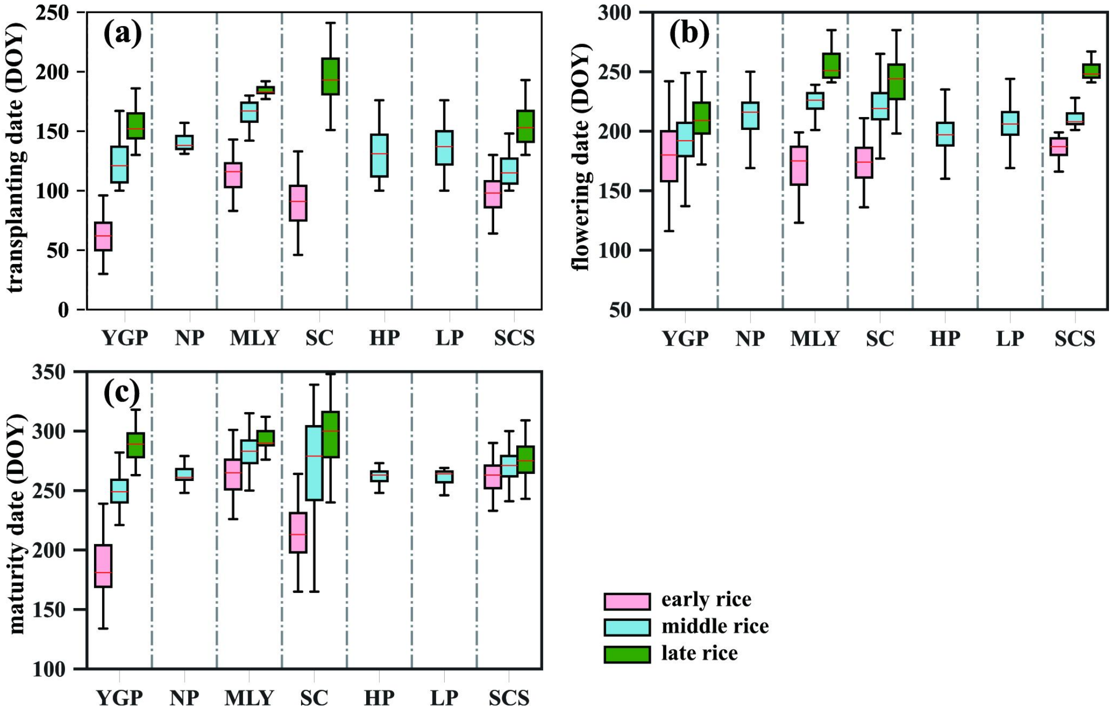

Fig.8 Rice phenological dates in main agricultural regions between 2003 and 2020 (a: Transplanting dates; b: Flowering dates; c: Maturity dates)

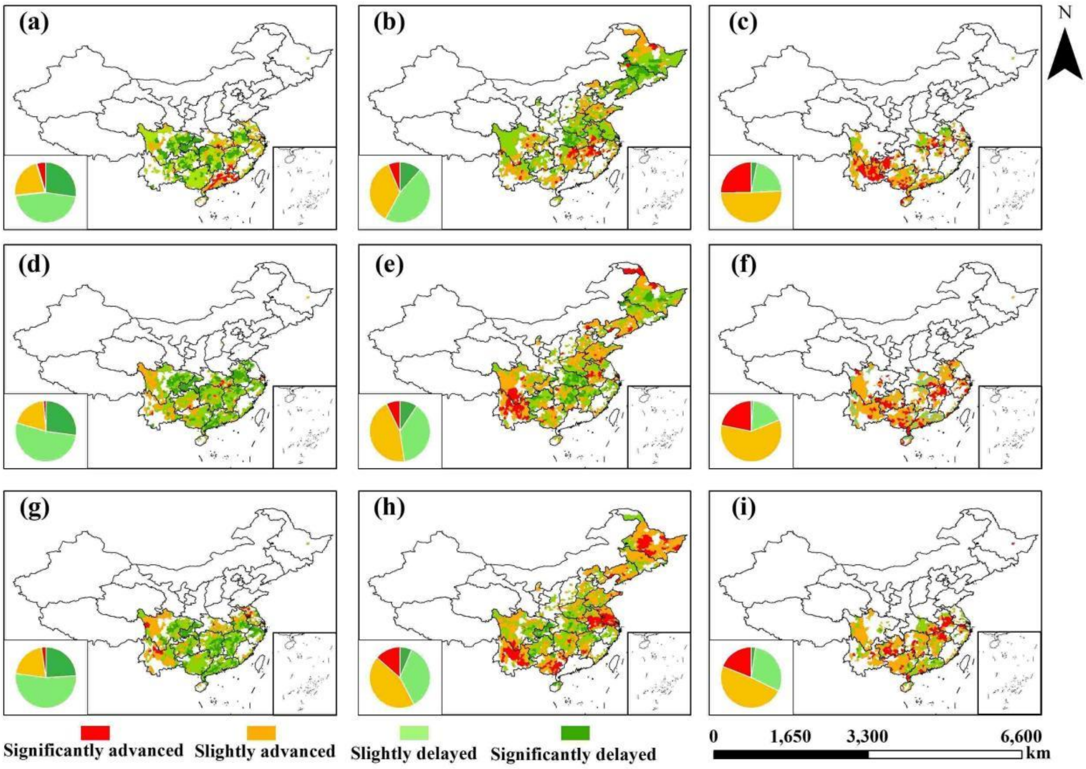

Fig.9 Temporal trends in rice phenological dates at the county scale from 2003 to 2020 (a: early-rice transplanting dates; b: middle-rice transplanting dates; c: late-rice transplanting dates; d: early-rice flowering dates; e: middle-rice flowering dates; f: late-rice flowering dates; g: early-rice maturity dates; h: middle-rice maturity dates; i: late-rice maturity dates)

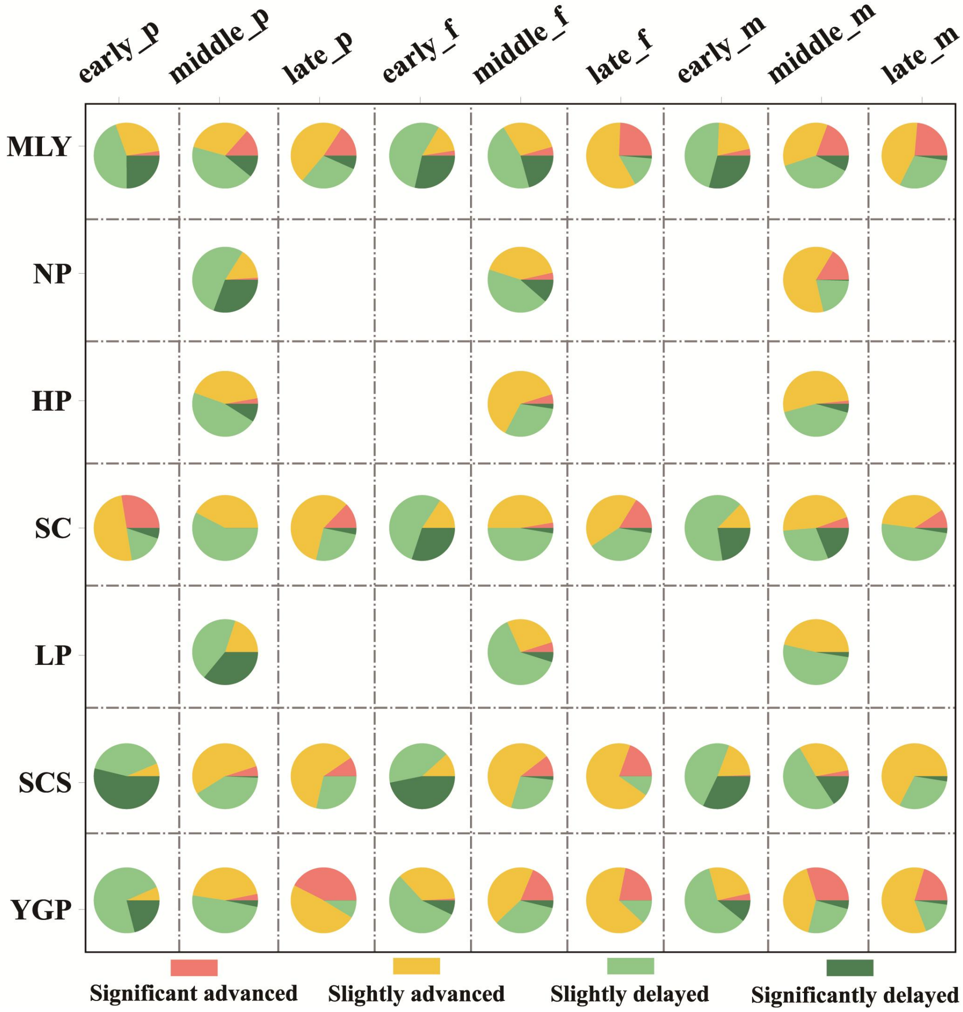

Fig.10 Temporal trends in rice phenological dates at the regional level from 2003 to 2020 (early_p: early-rice transplanting dates; middle_p: middle-rice transplanting dates; late_p: late-rice transplanting dates; early_f: early-rice flowering dates; middle_f: middle-rice flowering dates; late_f: late-rice flowering dates; early_m: early-rice maturity dates; middle_m: middle-rice maturity dates; late_m: late-rice maturity dates)

Table.1 PhenoRice parameters used in the study

Parameters	Value	Description
EVI_{avg_th}	0.40	threshold for the average EVI within the study period (< EVI_{avg_th})
EVI_{max_th}	0.50	threshold for the maximum EVI within the study period (> EVI_{max_th})
EVI_{min_th}	0.25	threshold for the minimum EVI within the study period (< EVI_{min_th})
vl1 (days)	40	shortest vegetative growth length
vl2 (days)	112	longest vegetative growth length
tl1 (days)	96	shortest total growth length
tl2 (days)	184	longest total growth length
LST_{th} (°C)	15	minimum land surface temperature for rice planting
Winfl (days)	24	time window for capturing flooding signals
minndfi	0	threshold for NDFI
Win_{decr} (days)	72	threshold for a decline window after EVI maximum
dec_{th}	0.50	percent decrease of EVI after EVI maximum

Table.2 R^2 between the detected and statistical rice area in main agricultural regions ($p < 0.05$)

	Early rice	Middle rice & single-season late rice	Double-season late rice
MLY	0.97	0.79	0.85
NP		0.95	
HP		0.94	
SC	0.92	0.73	0.78
LP		0.93	
SCS	0.89	0.82	0.79
YGP	0.90	0.77	0.89